EFFECT OF MAPK INHIBITION ON CELL CYCLE REGULATION OF

THYMIDINE KINASE 1 AND [^{18}F]-FLT PET

By

Nathan J. Mutic

Thesis

Submitted to the Faculty of the

Graduate School of Vanderbilt University

in partial fulfillment of the requirements

for the degree of

MASTER OF SCIENCE

in

Chemical and Physical Biology

December 2009

Nashville, Tennessee

Approved:

Professor H. Charles Manning

Professor John C. Gore

Professor Robert J. Coffey

Professor Hassan Mchaourab

Professor M. Kay Washington

This work is dedicated to my father, Stephen J. Mutic, and to the families whose lives

have been changed by cancer.

ACKNOWLEDGEMENTS

TABLE OF CONTENTS

Page

LIST OF FIGURES

Cell cycle regulation of thymidine kinase 1

Thymidine Kinase 1 (TK1) is a deoxyribonucleoside kinase which functions to phosphorylate and trap nucleosides following entry via facilitated diffusion through membrane bound nucloside transport proteins [1]. Since the TK1 gene was cloned in 1983 [2], an extraordinary body of work, enhancing our understanding of TK1 at transcriptional, translational, and post-translational levels has ensued. It is important to note that much of this work was performed in normal fibroblast cells, not cancer cells where many cell cycle control mechanisms are frequently dysregulated. TK1 protein levels and activity are governed by several independent molecular mechanisms. The gene promoter, containing two CCAAT motifs, GC and TATA elements, confers S phase specific transcription [3-5]. Specifically, the region located -441 to -63 nucleotides from the transcriptional initiation site is believed to be responsible for the S-phase specific initiation of transcription [6]. A previous study using intron specific PCR probes determined that in quiescent G_o fibroblasts heterogeneous nuclear TK1 mRNA was not detectable [6]. There also is evidence that S phase specific initiation of TK1 transcription is not only regulated by elements in the promoter region of the gene, but also by intragenic elements. This has been shown in differentiating cultured skeletal muscle cells [7]. Others have shown in experiments utilizing TK1 cDNA clones transfected into Rat-3 TK1-deficient cells that an intragenic region was capable of conferring cell cycle regulation of TK1 expression regardless of the promoter region studied [8]. Hence, not only does the gene promoter region code for S phase specific initiation, but also regions

within the coding portion of the gene function to do so as well. It is known that TK1, as well as many other S phase genes, are under the transcriptional regulation of the E2F transcription factor. Normally, E2F is bound by the hypophosphorylated Rb protein. Upon hyperphosphorylation by the cyclin D/cdk4/6 complexes and the cyclin E/cdk2 complex, Rb undergoes a conformational change and is released from the E2F transcription factor. This release of E2F allows for the initiation of TK1 transcription.

Beyond transcriptional regulation, further mechanisms ensure proper coordination of TK1 expression with the cell cycle. In normally cycling (non serum starved) HeLa cells, synchronized by centrifugal elutriation, TK1 mRNA increases less than three-fold from G1 to G2, where as in serum-stimulated cells, mRNA levels increase over 10-fold as cells begin to cycle [9, 10]. These results indicate that the mechanisms of transcriptional induction differ dramatically in normally cycling and serum stimulated cells [11]. In normally cycling cells, the three-fold increase in mRNA is accompanied by a 15-fold increase in the TK1 protein. This implies that translational efficiency is coordinated with cell cycle. The eIF4E protein plays a significant role in increasing translational efficiency in eukaryotic cells [12], and recent work by other members of our group has shown that eIF4E protein levels are elevated in DiFi cells immediately following treatment with C225 despite stable transcript levels (data not shown)

The activity of the protein has also been shown to increase in concert with cell cycle and is tightly linked to the amount of protein present [11]. With the commencement of DNA synthesis, TK1 activity levels increase [2]. TK1 protein levels increase shortly after the beginning of G1, continue to increase through G2 then decrease drastically after mitosis. Prior to cell division, the protein has a half-life of approximately 40 hours,

following cell division the half-life decreases to about 4 hours as determined with pulse chase experiments [11]. The post-translational mechanism responsible for TK1 degradation at the onset of G1 appears to be directed by carboxy terminus of the polypeptide. Removal of the C-terminal 40 amino acids or altering the C-terminal end of the polypeptide with a B-galactosidase fusion renders the protein stable throughout cell cycle [13].

The TK1 protein itself was purified in 1983 and identified to have an overall molecular weight of 92 kDa, and was comprised of two 44 kDa subunits [14]. The human TK1 cDNA is 1,421 base pairs long, and codes for a 25.5 kDa protein which, as determined by Southern blotting, is highly conserved across many vertebrates, showing greater than 74% amino acid homology between man and chicken [15]. The protein is capable of phosphorylating thymidine as a homo-dimer. However, it is fully functional as a homo-tetramer. ATP serves as a cofactor which allows two dimers to com together to form the fully functional tetramer. Formation of the fully functional tetramer is an ATP-dependent event. Structural studies of human and *Thermotoga maritime* TK suggest that ATP interacts with the TK enzyme between phosphate groups and the P-loop of the protein on residues 10-16 [16]. It is reasonable to hypothesize that this could have significant implications to 3'-deoxy-3'[^{18}F]-fluorothymidine ([18F]-FLT) Positron Emission Tomography (PET) imaging within the context of tissues with varying ATP profiles and therapies which can alter ATP level, though this effect is currently not known.

[18F]-FLT PET imaging as a biomarker for proliferation in cancer

A hallmark of cancer is unbridled cellular growth and proliferation. Proliferative assays are routinely performed *in vitro* and *ex vivo* as measures of cell proliferation and treatment response. *Ex vivo*, proliferation has been measured by incorporation of 5-bromo-2'-deoxyuridine (BrdU) or scoring Ki-67 positive cells [17, 18]. The main drawback of Ki-67 is the dependence on invasive biopsies. BrdU analysis only provides a static picture of the cells proliferation, is toxic, and requires that the animal be sacrificed to perform histological analysis of the tissue. Biopsies cause patient discomfort, further antagonize lesions, and confound serial biopsy and imaging readouts. The ability to non-invasively image proliferation *in vivo* with a quantitative biomarker such as [18F]-FLT, therefore has advantages over traditional, invasive procedures.

DNA synthesis occurs during S phase of cell cycle and is an essential step in proliferation. Two mechanisms are known for cellular DNA synthesis. Cells can produce thymidine from uridine precursors via the *de novo* pathway by methylation of deoxy-uridine-monophosphate (dUMP) by thymidine synthase (TS), or thymidine can be acquired from the environment via the via the salvage pathway. Theoretically, [18F]-FLT serves as a surrogate marker of proliferation by reporting the activity of thymidine salvage. The first step in the salvage pathway of DNA synthesis is transport of deoxyribonucleosides from outside the cell to the intracellular region. Next, nucleosides are monophosphorylated by a deoxyribonucleoside kinase. In the case of thymidine, this reaction is catalyzed by TK1. The resulting thymidine monophosphate is trapped within the cell by its negative charge (figure 1). Thymidine monophosphate is further processed before ultimately being incorporated into DNA either during S phase or routine DNA

repair. The former process provides the rational for [^{18}F]-FLT as a surrogate marker of proliferation. While [^{18}F]-FLT is phosphorylated, it is not incorporated into DNA as is thymidine, due to the functionalization at the 2' position (figure 1) [19-21]. Actively proliferating cells have increased demand for thymidine and are therefore usually detectable with [^{18}F]-FLT PET over less actively proliferating cells. It is important to note, however, that this is only true if the cell is dependent on the salvage pathway for DNA precursors.

[^{18}F]-FLT is an attractive biomarker for proliferation. Originally designed as an antiviral agent, [^{18}F]-FLT was abandoned because of side effects at therapeutic doses. Doses required for imaging are substantially lower, abrogating negative side effects. [^{18}F]-FLT is a very poor substrate for TK2, providing confidence in [^{18}F]-FLT as a measure of proliferation [22]. The two-hour half-life, relative ease of radiochemical synthesis, and lack of metabolic byproducts are all positive attributes of [^{18}F]-FLT. Thymidine is the only nucleotide required for DNA synthesis that is not utilized in the synthesis of RNA. Hence, the interpretation of retention of [^{18}F]-FLT cannot be confounded by contributions from transcriptional events.

Imaging of proliferation is not limited to the use of [^{18}F]-FLT, however, it has advantages over analogous imaging biomarkers. Other radiotracers indirectly related to proliferation have been used with some success including [^{11}C-methyl] TdR. ^{11}C TdR has been generally abandoned because of half-life constraints on ^{11}C, confounding metabolic byproducts, and the necessity to perform kinetic modeling [23]. TdR is also incorporated into mitochondrial DNA, confounding its interpretation as a biomarker of proliferation. [^{18}F]-FLT has been used successfully in many clinical and preclinical settings. [^{18}F]-FLT

has been compared to [^{18}F]-FDG, used as a surrogate of biological events other than proliferation, correlated with TK1 protein levels in tumors, and TK1 activity [24] [25] [26] [27]. One of the strongest motives for imaging proliferation is that therapeutically induced changes in proliferation may precede changes in tumor volume measured by other metrics such as CT, MRI, or US. It has been reported that changes in [^{18}F]-FLT PET imaging precede changes in tumor volume as a result of gefitinib treatment in patients with lung cancer [21].

Effect of EGFR targeted therapies on TK1 levels

One aspect of [^{18}F]-FLT PET that requires further investigation is the relationship between [^{18}F]-FLT retention and TK1 protein and activity levels prior to and following cancer therapy. The increasing emphasis on development and use of molecularly targeted therapies underscores the importance of validating imaging biomarkers within clinically relevant, yet frequently complicated settings. The epidermal growth factor receptor (EGFR) has shown promise as a target for molecular therapies in head and neck, lung, and colorectal cancers [17, 19 22-24]. Blockade of the EGFR signaling axis with small molecule tyrosine kinase inhibitors (TKIs) and therapeutic monoclonal antibodies affects signaling cascades and the transcription of genes, which regulate TK1 enzyme levels. Only through proper validation, in appropriate contexts, can we begin to understand the implications of molecularly targeted therapies on imaging readouts.

The EGFR is capable of transmitting extracellular signals, in the form of one of 7 known ligands, to intracellular signals [28], Among the most important EGFR ligands in CRC are TGF-α and amphiregulin [29]. The two primary pathways of EGFR signaling

are the AKT and MAPK signaling cascades (figure 2). These two pathways are ultimately responsible for transcription of specific genes involved with proliferation, angiogenesis, resistance to apoptosis, and other cellular events. An understanding of how modulation of these pathways can affect TK1 expression is critical for proper interpretation of [^{18}F]-FLT PET imaging data, especially in the context of therapies that may affect the MAPK and AKT signaling networks.

MAPK is responsible for phosphorylating and activating a number of gene expression regulatory molecules. The MAPK cascade can lead to phosphorylation and stabilization of the p53 tumor suppressor protein. When phosphorylated, p53 is released from MDM2 and therefore no longer targeted for degradation. The p53 protein, upon translocation to the nucleus induces expression of p21, a negative regulator of cell cycle and TK1 expression. The p21 protein can bind to and inhibit cyclin cdk2/4 complexes from phosphorylating Rb thereby inducing a G1 arrest. Logically, reducing MAPK activity via EGFR blockade should affect the [^{18}F]-FLT PET signal by imposing G1/S arrest and therefore reducing the amount of TK1 transcription. MAPK also phosphorylates FoxO3a, thereby targeting it for degradation. FoxO3a, in its unphosphorylated state, is targeted to the nucleus and enhances transcription p27 and Bim [30] (figure 2). The p27 protein is another negative regulator of cell cycle and, of importance to [^{18}F]-FLT PET imaging, can reduce levels of TK1 through G1/S arrest.

Though not the central focus of this study, we recognize that PI3K signaling is important in CRC. AKT is involved in a number of signaling cascades which commonly regulate processes such as survival and motility. Interestingly, it has been demonstrated that attenuating AKT activity either by expressing dominant negative forms of the protein

or by treatment with chemotherapeutics such as cisplatin leads to reductions in p21 levels [31]. AKT has a similar role in FoxO3a regulation as MAPK [30]. One primary difference in MAPK and AKT regulation of FoxO3a is in their ability to phosphorylate FoxO3a at specific sites. AKT specifically targets Thr 32, and Ser 253 and 315. MAPK, however has been shown to specifically target Ser 294, Ser 344 and Ser 425 which leads to subsequent translocation of FoxO3a to the cytoplasm. Work by Yang et. al. indicates that mdm2 is very likely to be the ubiquitin ligase responsible for degradation of FoxO3a following its phosphorylation [32]. Therefore we envision that elucidation of much of how PI3K signaling affects TK1 regulation is also a very important future endeavor.

Preclinical model

DiFi cells originated from a patient with familial adenomatous polyposis and were first developed by Dr. Boman [33]. DiFi cells express wild type KRAS, and express very elevated levels of the EGFR [18, 33]. It has been suggested by others that DiFi cells harbor a mutant p53 allele [33] and our work supports this hypothesis. Based upon their KRAS and EGFR status, they are expected to be a cetuximab-sensitive CRC line, which we [18] and others [34] have shown in previous studies. As p53 is primarily responsible for regulating transcription of p21 and KRAS is the protein in the ERK pathway, these two mutations are extremely important in regulating the proliferative activity of the cell. Approximately 80% of CRC tumors and 50% of all other known tumors have mutations in one or both of their p53 alleles, therefore the DiFi line is a relevant model for these studies. In some cases, as a control, we also studied HCT116 cells, which express mutant KRAS but wild type p53, and EGFR[18]. Using these model lines affords the capacity to

identify molecular events that control levels of TK1 and ultimately the [18F]-FLT PET signal in p53 mutant and wild type cell lines.

RESULTS

[18F] FLT PET reflects TK1 levels at the protein and mRNA levels

Static [18F]-FLT PET images were acquired from HCT116 (figure 4A) and DiFi (figure 4B) xeograft-bearing nude mice. The HCT116 cell line grows considerably faster than the DiFi line as xenografts *in vivo* [18] *and in vitro*. Significantly greater tracer retention is observed in HCT116 xenograft tumors compared to DiFi tumors. We quantified this difference in terms of percent-injected dose per gram (%ID/g). As shown in figure 1C, the average %ID/g measured in HCT116 mice was 8.82, n=23, and 3.80 in DiFi tumors n=37. Using dynamic PET scanning, it is possible to determine various rates of specific events of [18F]-FLT metabolism. FLT PET data acquired in mice can be fit to a three compartment (vascular space, exchangeable [18F]-FLT within the tissue, and trapped [18F]-FLT within the tissue) tracer kinetic model. In this model, four rate constants are used to describe; the transport of [18F]-FLT into the cell from the vascular space (k_1) (delivery), the reverse process of the tracer leaving the tissue and entering the vascular space (k_2) (efflux), phosphoralation and trapping of [18F]-FLT in the cell (k_3), and dephosphorylation of [18F]-FLT (K_4) [35]. Another member of our group, Eliot T. McKinley working on this type of kinetic modeling determined that the differences observed in static scans were also reflected in the k_3 measures from cohorts of HCT116 and DiFi xenograft tumors which were 0.063 min^{-1} n= 6 and 0.027 min^{-1} n=8,

respectively (figure 4D). This difference in k_3 values indicates that rate of phosphorylation and ultimately retention of FLT in HCT116 tumor cells is much greater than in DiFi cells and implies that TK1 is likely much more active or more abundant in HCT116 cells. Importantly, the differential tracer retention observed in these two tumor types was reflected in levels of TK1 protein and transcript *in vitro* as measured by western blot and qRT-PCR (figure 4E). We noted that levels of TK1 protein were significantly lower in DiFi cells than in HCT116 cells. The correlation between [^{18}F]-FLT PET data and western blot data of TK1 protein levels or qRT-PCR data of mRNA was roughly one to one (data not shown). This correlation was not surprising as TK1 is responsible for phosphorylating [^{18}F]-FLT leading to its inability to diffuse back across the cell membrane.

Histological analysis of tumor cell cycle distribution

We also performed histological analysis of the two tumor types to assess differences in cell cycle distribution and to assess the relative proliferative activity of each line studied. We examined a number of histological markers of proliferation which each detect distinctly different phases of cell cycle. As TK1 expression is tightly regulated with cell cycle, we believe it is critical to examine a number of histological markers which mark unique events which occur at specific times during cell cycle. As shown in figure 5, no appreciable difference was observed in Ki-67, or phosphorylated histone H3 staining of HCT116 or DiFi tumor samples. The percent positive nuclei per field for PCNA staining were significantly greater ($p < 0.0001$) for HCT116 compared DiFi tumors. Ki-67 marks cells in any non-G0 phase of cell cycle. The phosphorylation

of histone H3, which specifically occurs during chromosome condensation in mitosis and meiosis [36] marks cells specifically in M phase. The proliferating cell nuclear antigen (PCNA) stain detects levels of the DNA ring protein which is primarily involved in regulating DNA synthesis and repair events [37] hence PCNA marks cells specifically in S phase. These data suggest that the difference in cell cycle distribution between these two tumor types is primarily in the proportion of cells in S phase which agrees with the distinctly different patterns of FLT data in each line.

EGFR blockade with C225: attenuated MAKP and AKT signaling in DiFi cells

To assess the effect of C225 on MAPK signaling, cell cycle regulatory molecules, and ultimately TK1 levels in DiFi cells, we treated cells *in vitro* with either 0.5 or 5.0 ug/ml of C225 over a 48 hour time course (figure 6). Cells grown on plastic tissue culture dishes in the presence of growth factors were treated. Since TK1 is tightly regulated during cell cycle, it was important that we not serum starve cells in our experiments. Initially, we evaluated levels of total EGFR and phosphorylated EGFR at tryosine residues 1148 and 1178. By two hours post-treatment at 5.0 ug/ml, there was a marked reduction in total EGFR. Levels of total EGFR continued to decline for the remainder of the time points measured indicating that the receptor was likely being internalized and degraded. At the low dose, however, levels of total EGFR fluctuated only moderately throughout the experiment. At the high dose C225, levels of phosphorylated EGFR at tyrosine 1148 increased dramatically one hour following treatment then returned to baseline levels by 24 hours after treatment. At the same dose, we observed a steady increase in levels of EGFR phosphorylated at tyrosine residue 1173 throughout the time

course. While levels of phospho-EGFR tyr 1173 appeared to increase, it is likely this was a concentrative process occurring because of reduced total EGFR levels. Levels of both of these residues fluctuated slightly throughout low dose experiment. We next assessed levels of proteins associated with the MAPK and AKT signaling networks, which can be under control of EGFR.

The MAPK signaling axis, which translates extracellular signals in the form of growth factors into intracellular signals, which govern the cells proliferative activity, is directly linked to the EGFR. After recruitment of the cytosolic protein Sos by an adaptor protein, Grb2, to the cytoplasmic domain of the EGFR, RAS can be activated which initiates the MAPK signaling cascade. Levels of total RAS were not significantly altered by treatment with either dose. Levels of phosphorylated MEK 1/2 at Ser 217/221 was decreased after one hour of treatment and remained at lower levels until 48 hours when they returned to normal at both concentrations. The next protein in the MAPK cascade probed was phosphorylated p44/42 ERK 1/2 at Thr 202 and Tyr 204. At the low concentration there was a distinct fluctuation in levels of throughout the experiment. However, at 5.0 ug/ml there was a drastic decline in phospho p44/42 ERK 1/2 after one hour of treatment that persisted until 48 hours post-treatment. Levels of phospho p44/42 ERK 1/2 were undetectable from the one hour to 24-hour time points. We interpreted the return in activated ERK at 48 hours in the higher dose as a consequence of the C225 being used up. Relevant to TK1 regulation, activated ERK is responsible for influencing a number of gene expression profiles, specifically, the G1 cyclins. As shown below, reduction of G1 cyclins can lead to hypophosphorylation of Rb and subsequent reduction in TK1 transcription. It is important to reiterate here that the DiFi cell express very high

levels EGFR, so it is reasonable to assume that this line may be reliant on EGFR

regulated signaling pathways such as MAPK and potentially PI3K. Another relevant

target of MAPK is the transcription factor, FoxO3a which when unphosphorylated

translocates to the nucleus and regulates a number gene expression patterns including p27

and Bim.

We also assessed levels of proteins relevant to the AKT signaling axis. Levels of

total AKT were unaltered at either dose tested. Both phospho residues tested, Thr 308 and

Ser 473, showed little change throughout the experiment with the exception of a distinct

peak at the eight-hour time point. At the 5.0 ug/ml, however, both phospho residues were

substantially attenuated after only one hour of treatment and remained lowered until 48

hours when phospho-AKT Thr 308 was elevated slightly, but not back to baseline levels

and phospho-AKT Ser 473 was elevated back to baseline levels. Activated AKT

promotes cell growth and survival by activating proteins such as mTOR and many others

leading to increased glucose catabolism, protein synthesis, and membrane biosynthesis.

Shutting down AKT ultimately abrogates these types of growth and survival signals.

C225 induces G1/ S arrest in DiFi cells mediated by p27

DiFi cells were treated with 0.5 ug/ml and 5.0 ug/ml doses of C225 *in vitro* and

harvested over a time span from 0 to 48 hours to assess levels of proteins involved in the

G1/S cell cycle checkpoint (figure 7). As TK1 is ultimately under the transcriptional

regulation of Rb, we were specifically interested in how the levels of cell cycle promoters

and inhibitors were altered after treatment with C225. As expected, only after a

stochiometric shift was observed in favor of cell cycle inhibitory proteins did levels of phosphorylated Rb decline and TK1 drop as well.

At the higher dose, levels of cyclin D1 increased from baseline until after 8 hours of treatment at which point they dropped to almost baseline levels. By 12 hours of drug exposure, they were at undetectable levels and remained down until 48 hours post treatment. Cyclin D3 levels increased dramatically from 2 to 8 hours after treatment then dropped to baseline levels by 12 hours and were undetectable at 24 and 48 hours of drug exposure. Both cyclin D1 and D3 protein levels showed similar but more modest fluctuations from baseline levels when treated with the 0.5 ug/ml dose of C225. Cyclin D3 protein levels increased steadily from 1 to 24 hours until returning to baseline at 48 hours. Cyclin E (which governs progression through the R point) levels were unaltered from baseline until after 8 hours of treatment at the effective dose when they dropped significantly and remained down for the rest of the experiment. At the lower concentration, we observed an initial reduction of cyclin E protein levels after one hour, which persisted until 24 hours after treatment. Next, levels of relevant cyclin dependent kinases were assessed. Cdk4 and Cdk6, when bound to cyclin D, can become activated and activate a number of G1 specific proteins via phosphorylation. We noted that following treatment with the 5.0 ug/ml dose of C225, levels of Cdk4 increased slightly from 2 to 8 hours after treatment then declined consistently after 12 hours of drug exposure. Levels of Cdk6, the other cyclin D binding partner remained unchanged at either dose tested. We also probed levels of Cdk2, the G1/S transition kinase that partners with cyclin E. We observed little change in levels of Cdk2 protein following treatment with the lower concentration. Interestingly, at the elevated dose, we noted a temporary

marked reduction in Cdk2 protein levels at the two-hour time point that coincided with temporary attenuation of phosphorylated Rb levels at serine 807/811. Levels of Cdk2 increased slightly at the four-hour time point, then declined steadily for the rest of the experiment. Generally, what we observed in relative levels of G1 and G1/S transition cyclin and corresponding Cdk proteins was a minor fluctuation at the lower dose of C225 and a marked reduction after 8 hours at the higher dose.

We probed various Cdk inhibitory (CDKI) protein levels. Levels of the INK4 family p15 and p16 were assessed as well as levels of p21 and p27. CDKI proteins function by binding the activated cyclin-Cdk complex and allosterically inhibiting the ATP-binding active site of the Cdk. We did not observe a change in levels of both INK4 family CDKIs assessed (p15 or p16) at either dose tested. Levels of p21, however, declined dramatically after eight hours of exposure at the high dose, were increased modestly at 24 hours from baseline, then declined to almost undetectable levels by 48 hours. These observations on levels of p21 protein levels following C225 treatment appear consistent with the DiFi line harboring a p53 mutation because of the modest p21 response. Interestingly, this coincided temporally with levels of p53 phosphorylated at Ser 15, indicating that the activated p53 observed was functional and capable of inducing a p21 response when present (figure 10).

The p27 response was more dramatic than the p21 response. Levels of p27, however, increased slightly after only one hour of treatment then increased again dramatically after 24 hours. This coincided temporally with levels of phosphorylated FoxO3a (residue 253 or 32). When dephosphorylated, FoxO3a can translocate to the nucleus and promote transcription of the *CDKN1B* gene. With careful observation of the

balance between Cdk2 and p27, it is appears that transient reduction in Cdk2 protein

levels at two hours corresponds temporally to the increases in p27 levels. Moreover, the

decrease in Cdk2 levels from four hours on corresponds to a similar increase in p27

mRNA levels early on and protein levels by 24 hours. This agrees well with the known

ability of Cdk2 to phosphorylate p27 that leads to recognition of p27 by the F-box protein

and subsequent ubiquitylation (and ultimately degradation) by the S-phase kinases-

associated protein 1-cullin-F-box containing protein complex (SCF). Generally, it

appeared the INK4 proteins, which govern activity of the cyclin D/Cdk4/6 complexes

early in G1 showed a much less robust response to C225 than did p27. Ultimately we

observed that only after a dramatic reduction in cyclins D2, D3, and E, as well as Cdk 2,

4, and 6 with a concomitant increase in levels of p27 specifically, did we note a drastic

reduction in phosphorylated levels of Rb at serine 807/811. As Rb is a primary

transcriptional regulator of the TK1 gene we, as expected, noted that levels of TK1

became undetectable from 24 hours after treatment at the higher concentration of C225.

p27 SiRNA

To determine the specific effect of levels of p27 on TK1, we knocked down levels

of p27 protein with SiRNA both in the presence or absence of 5.0 ug/ml C225 (figure 8).

For both cases, with or without drug, we also tested the effect of a random SiRNA

sequence on levels of p27 and TK1 protein. We found that that in all cases where drug

was absent, there was a low baseline level of p27 present. We noted that TK1 levels were

elevated in cells not exposed to drug but given either random or p27 siRNA. We have

seen elevated TK1 levels in previous experiments (data not shown) when cells are serum

starved or at low serum levels. This may indicate a conflicting response to the random

sequence used in this experiment and is under further study. As per manufacturer's

instructions all SiRNA treated cells were grown in 3% serum verses the normal 10%

serum levels. We speculated that the increase in TK1 seen in the cells given random or

p27 SiRNA, but no C225 was attributed to these low serum conditions. After 24 hours of

C225 exposure, we noted the expected increase in p27 and slight decline in levels of

TK1. We observed an expected increase in p27 protein levels in C225 treated cells

exposed to a random SiRNA. In that case, TK1 was also elevated and we believe this is

most likely due to low serum levels. As predicted, when cells were exposed to C225 and

p27 SiRNA there was no increase p27 and TK1 levels remained just above baseline

levels. These data suggest that p27 is responsible for the attenuated levels of TK1

observed in the presence of C225.

qRT-PCR for TK1 and p27

To determine whether the decline in TK1 levels following C225 treatment was

originating at a transcriptional or translational level we assessed mRNA levels of p27 and

TK1 by qRT-PCR every three hours over a 24 hour time course (figure 9) (protein lysates

were also generated for direct comparison to mRNA data (data not shown)). We noted a

small constant decline in TK1 mRNA from the six hour time point until 18 hours of drug

exposure at which point the mRNA levels declined drastically until 24 hours of drug

exposure. Given the drop in mRNA occurs at or prior to the decline in TK1 protein, these

data suggest that the primary mechanism of TK1 protein reduction does not stem from a

decline in transcriptional efficiency or an increase in protein degradation but rather through transcriptional regulation.

We also measured mRNA levels of p27 at three-hour intervals from zero to 24 hours. We initially saw a slight increase in p27 mRNA levels following treatment from one to three hours. At the six-hour time point we noticed a drastic reduction in mRNA from baseline of roughly two-fold. After the six-hour time point, and until 21 hours of drug exposure, mRNA levels fluctuated from one to four-fold over baseline levels. From 21 hours to 24 hours of drug exposure, levels of mRNA dropped to roughly one and a half fold below baseline.

AG1478 and C225, link between p27 and TK1

To determine if the aforementioned responses were limited to growth factor withdraw induced by C225 or if they were also relevant to EGFR inhibition, we tested the effects of the small molecule tyrosine kinase inhibitor AG1478. DiFi cells were treated with 1.0 uM or 100 nM AG1478 or 0.5 ug/ml or 5.0 ug/ml C225 as single agents (figure 10), ordered (not shown), or in combination (not shown). Levels of cyclin D1, cyclin D3, Cdk4, Cdk6, p27, and TK1 protein confirm our previous experiments with C225 with a distinctly different therapeutic agent at either the dose tested. Interestingly, 24 hours after treatment with 1 uM AG1478, we noticed the same relationship between p27 and protein levels of TK1 as observed with the 5.0 ug/ml dose of C225. However, there was a much smaller reduction in cyclin D3 levels and almost no reduction in cyclin D1 levels. These observations are consistent with AG1478 acting as a tyrosine kinase inhibitor and not as an agent that blocks ligand engagement with EGFR. The decline observed in cyclin levels

is consistent with growth factor withdrawal induced by C225. Levels of Cdk4 and 6 were unaltered. A substantial increase in TK1 protein occurred after 24 hours of exposure with 100 nM AG1478, however, no appreciable change was noted in the levels of any other protein tested. Importantly, from this experiment we observed the inverse relationship between p27 and TK1 held regardless of where EGFR was inhibited. The primary difference between the two drugs given as single agent was their ability to reduce cyclin levels.

Transcription factor analysis

Levels of total p53 protein remained constant following treatment with 5.0 ug/ml C225 (figure 11). Phosphorylated p53 protein levels increased from 1 to 4 hours after treatment relative to baseline and were undetectable at any later time point. Levels of p21 protein dropped by 8 hours of treatment. These data are consistent with the role of phosphorylated p53 positively regulating transcription of p21 as we observed a decline in levels of phosphorylated p53 after 8 hours of treatment as well. We also measured total levels of the transcription factor FoxO3a, which remained constant, and two distinct phosphorylated residues of FoxO3a. FoxO3a is a known p27 transcription factor. There was a distinct drop in the level of phosphorylated FoxO3a at the Thr 32 residue at the 24 hour time point. This drop occurred in concert with a marked increase in p27 protein levels at that same time point. FoxO3a is also known to induce transcription of Bim when dephosphorylated. Accordingly, levels of phosphorylated FoxO3a at the serine 253 residue dropped consistently over time, while levels of Bim increased steadily from 1 to 24 hours of treatment. This observed decline in phosphorylated FoxO3a agrees well with

the attenuation of activated MAPK and AKT levels observed previously, as FoxO3a is a known target of MAPK and AKT. We noted that there appeared to be some degree of specificity for the ability of the two phosphorylated residues tested to control the transcription of either p27 or Bim. As noted earlier, levels of Bim increase steadily *in vitro* following treatment with effective doses of C225 (figure 11). Bim is a BH3-only-domain protein that binds and neutralizes members of Bcl-2 pro-survival proteins, thereby allowing the proapoptotic proteins such as bad and bax to promote apoptosis. We observed steady increase in the amount of Bim_{EL} following treatment. We also observed a drastic reduction in the levels of activated Erk1/2. Erk1/2 is known to phosphorylate Bim_{EL} and target it for proteosomal degradation.

Colocalization of p27 and FoxO3a in C225-treated DiFi Cells

We preformed confocal microscopy to validate that the increase in p27 protein levels observed at 24 hours post C225 treatment by western blot represented functional nuclear p27 compared to inactive cytosolic p27. The p27 protein is known to only be capable of inducing cell cycle arrest when localized to the nucleus [38]. As shown in figure 12A, p27 in C225 (5.0 ug/ml) treated DiFi cells is localized in the nucleus after 24 hours of drug exposure. Untreated DiFi cells show low levels of p27 dispersed evenly throughout cytoplasmic and nuclear portions of the cell. We evaluated DiFi cells to confirm that FoxO3a was nuclear following 24 hours of 5.0 ug/ml C225 As seen in figure 12B, the distribution of FoxO3a within the cell was concentrated in the nucleus following 24 hours of C225 exposure. These studies confirm the western blot experiments suggesting that cell cycle regulation of TK1 is FoxO3a, p27-dependent in these cells.

[^{18}F] FLT PET reflects TK1 levels in an in vivo treatment model

DiFi xenograft bearing mice were treated with vehicle, 0.5 mg, and 1.0 mg C225 to assess the ability of [^{18}F]-FLT PET to measure changes in proliferation in an *in vivo* treatment model. Tumor-bearing mice were imaged pre-treatment on day one, then treated with vehicle, 0.5 mg, or 1.0 mg C225 on days two, four, and six. The mice then underwent their post-treatment PET image on day 7. The [^{18}F]-FLT PET signal decreased in a dose-dependent manner (figure 13). This decrease was not significant between vehicle and 0.5 ug/ml ($p > 0.05$) but was between vehicle and 1.0 ug/ml ($p < 0.001$). We extrapolated from this data that the dose-dependent attenuation of tracer retention reflects the same dose-dependent effects observed in the molecular mechanisms governing TK1 expression *in vitro*.

DISCUSSION

The goal of this work was to evaluate the effect of oncogenic signaling pathway inhibition with EGFR blockade on TK1 expression and ultimately the [^{18}F]-FLT PET. [^{18}F]-FLT PET has been frequently described as a biomarker of proliferation. The term proliferation refers to the normal combined process of cellular growth and division. These processes are often dysregulated in cancer. Therefore, it is essential to study the molecular mechanisms that control these processes in parallel with [^{18}F]-FLT PET imaging studies to fully appreciate the value of the tracer as a biomarker of proliferation. While the TK1-dependent phosphorylation of [^{18}F]-FLT resulting in its retention is well

understood [20], few studies have explored the effect of signaling pathway activity in cancer on TK1 regulation.

We show here that under certain conditions, [18F]-FLT PET can be interpreted as an accurate measure of proliferation. For example, we observed a strong agreement between [18F]-FLT retention and proliferative capacity by measuring tracer uptake in static and dynamic scans in a two cell lines with distinctly different growth rates(fig 4). These imaging results showed a one to one agreement with levels of TK1 at the protein and mRNA levels as measured by western blot and qRT-PCR.

While many have used Ki67 staining as an independent measure of proliferation to correlate with [18F]-FLT tracer retention, we found Ki67 to be a poor, and even misleading, correlate with FLT PET. While the two lines studied here were clearly variable in their growth rates and FLT retention, Ki67 staining did not reflect these differences. It is important to recognize that the Ki67 antigen is present at all non-G0 phases of cell the cycle. This contrasts greatly with the expression profile of TK1, which catalyzes the rate-limiting step of [18F]-FLT retention, phosphorylation of [18F]-FLT. Given that TK1 expression is normally confined to S phase, we compared the proportion of PCNA-positive cells. As expected, the trend seen in our PET data was reflected histologically with an S phase specific antigen. This correlates with our PET data, and supports the notion that [18F]-FLT PET is specifically an indicator of TK1 activity.

After verifying the association between proliferation, TK1, and [18F]-FLT retention in our model cell lines, we assessed ability of [18F]-FLT PET to assess treatment response *in vivo*. We chose DiFi, a cetuximab-sensitive line to assess the ability of [18F]-FLT PET to detecte responses to C225. We have shown previously that DiFi xenografts

undergo apoptosis and regress in response to C225 [18] at a dose of 0.5 mg/dose. In that work, we determined that the primary mechanism of action of cetuximab in DiFi xenografts was apoptosis, not a reduction in proliferation. No changes were observed in [^{18}F]-FLT PET *in vivo,* yet NIR-annexin-5 uptake correlated with caspase-3 activation and tumor regression. We have, however, shown here that utilizing a larger dose, a measurable reduction in tracer retention occurs. This dose-dependent response prompted further investigation of the dose dependent response in tracer retention to cetuximab that was evaluated *in vitro* in this study.

Our initial assessment of EGFR inhibition by western blot revealed that cetuximab was effective at 5.0 ug/ml at reducing levels of EGFR, we suspect by inducing degradation of EGFR, but not at an lower dose of 0.5 ug/ml. As expected, little change in phosphorylated tyrosine 1148 or 1153 residues was observed at the low dose of C225. However, at high dose Tyr 1148 decreased with total EGFR levels, while Tyr 1153 appeared to increase. The reduction in EGFR was accompanied by a dramatic attenuation of both activated MAPK and AKT. Both activated AKT and MAPK are known to be responsible for degrading Bim [39], a pro-apoptotic member of the BH3 only domain proteins. The early and dramatic attenuation in activated MAPK following C225 may partially explain the detectable apoptotic response seen in the DiFi cells that preceeds induction of p27 and loss of TK1.

It is evident from these studies that C225 induces G1 arrest that is p27-dependent and independent of p21 and INK4 responses. We observed a modest induction of p21 followed by a loss in p21 after treatment with C225. Levels of p27, however, increased over time. This rise in p27 occurred concomitantly with a decline in cyclin D1, D3 and E.

Not until a stochiometric shift toward an increase in negative and decrease in positive cell cycle regulators was achieved did we observe drastic reductions in levels of phosphorylated Rb Ser 807/811, which led to loss of TK1 protein. In response to C225, confocal microscopy confirmed that the p27 observed was nuclear and colocalized with FoxO3a.

Coupling the loss of p21 and gain of functional p27, we surmised that the FoxO3a transcription factor might be responsible for the C225-induced loss of TK1. Interestingly, MAPK and AKT, which were both deactivated with treatment, are responsible for phosphorylating and degrading FoxO3a. Only after dephosphorylation of FoxO3a did we notice an increase in p27 or Bim. The nuclear localization of FoxO3a following treatment with C225 further validated its role in the induction of p27 transcription.

To further validate the role of p27 in TK1 reduction, we preformed two additional experiments. One experiment showed that knocking down levels of p27 with SiRNA led to sustained levels of TK1, even in the presence of C225. We also demonstrated that following treatment with C225, levels of p27 transcript increased prior to a marked reduction in TK1 at the protein level. Ultimately, these data demonstrate the mechanistic link between C225 induced inhibition of MAPK and AKT signaling and p27-dependent reduction of TK1 protein levels.

In this work, we have established mechanistic evidence for the attenuation of [^{18}F]-FLT tracer retention in a p53 mutant, wild type KRAS CRC line that is responsive to EGFR blockade with C225. This work lays the foundation for further investigation of biological events governing [^{18}F]-FLT retention within the context PI3K inhibition as well as other oncogenic pathways that may include Src kinase. Future studies should

include dual pathway inhibition of MAPK, PI3K, as well as blockade of other important

Hers such as Her3.

CONCLUSIONS

Regulation of TK1 is very complex and has implications on interpretation of

$[^{18}F]$-FLT PET data. $[^{18}F]$-FLT PET can be used as a surrogate marker of tumor cell

proliferation with knowledge of its important limitations. We have demonstrated here that

a tighter correlation exists between PCNA staining and $[^{18}F]$-FLT retention compared to

Ki67 staining. We have also established the role of MAPK and AKT inhibition leading to

FoxO3a signaling in TK1 regulation in a p53 mutant cell line. Our data shows that

inhibition of oncogenic MAPK signaling with EGFR targeted therapy leads to reduced

TK1 levels in a p27, FoxO3a-dependent manner. In a p53 wild type cell line, p21 may

also play an important role as well as the INK4s. Regulation of TK1 in turn leads to a

reduction in $[^{18}F]$-FLT tracer retention.

METHODS

Mouse modeling

DiFi and HCT116 xenografts were generated in athymic nude mice (Harlan

Sprague Dawley) following subcutaneous injection of 2-4 $x10^6$ cells. Palpable tumors

were typically detected within 2-4 weeks.

Radiopharmaceuticals

[^{18}F]-FLT was prepared by the Vanderbilt University Radiochemistry Shared Resource according to published procedures [18].

In vivo imaging

All studies involving animals were conducted in compliance with federal and institutional guidelines. DiFi and HCT-116, xenografts were generated in athymic nude mice (Harlan Sprague-Dawley) following subcutaneous injection of $2x10^6$ to $4x10^6$ cells. Palpable tumors were detected within 2 to 4 weeks. For treatment studies, tumor-bearing mice (0.5-1.0 cm longest dimension) were administered cetuximab (40 mg/kg) or saline vehicle intraperitoneally every 3 days for 1 week (three total injections). Following anesthesia (2% isoflurane in O2 at 2 L/min), animals were administered 180 to 200 uCi [^{18}F]-FLT via intravenous injection before imaging on a Concorde Microsystems microPET Focus 220 (Siemens Preclinical Solutions). Animals remained conscious and were allowed free access to food and water during a 1 hour uptake period. For PET scanning, mice were anesthetized (2% isoflurane in O2 at 2 L/min) and imaged in the prone position for 15 min. Body temperature was maintained before and during imaging using a thermostat controlled circulating warm water pad. Immediately following imaging, both treated and untreated mice were sacrificed, and tissues were collected for histopathologic, western blot, and qRT-PCR analysis for validation purposes.

Tissue culture

DiFi and HCT116 cell lines were maintained in DMEM media (Cellgro, Herndon, VA, USA) supplemented with 10% fetal bovine serum (FBS) (Invitrogen 26140, Grand Island, NY, USA) and 1.0% penicillin streptomycin (PS) cocktail at 37 °C in an atmosphere of 5% CO_2 with constant humidity levels. Media, tripsin, and DPBS was warmed to 37 ^{0}C in a water bath before application to cells. Cells were checked with a microscope to ensure all cells were 70% confluent at the time of *in vitro* experiments. All cells used in experiments were passed fewer than 20 times. Sterile technique was used at all times while passing cells in a laminar flow sterile tissue culture hood and all plates were checked visually for contamination. Particular precaution was taken to spray all plates, media containers, and instruments with 70.0 % ethanol prior to putting them into the hood. To pass cells, the growth medium was first removed by aspiration, being careful not to disturb the adherent cells. Next, cells were washed with warmed sterile DPBS prior to addition of two ml of 0.25% trypsin. After addition of trypsin, plates were returned to the incubator and checked temporarily for detachment of cells. Careful precautions were taken to assure that all cells were non-adherent prior to passing in order to assure all cells an equal likelihood of propagation. Warmed media (8 ml) was then added to the 2 ml of tripsinized cells. The total 10 ml of cell suspension was then rinsed over the plate at least 10 times to ensure cells were completely detached from the plate. Next, 2 ml of cell suspension was then added to a clean plate with 8 ml DMEM media supplemented with 10% FBS and 1.0% PS, then returned to the incubator.

In vitro treatment assays

All cells used in treatment assays were grown to 70% confluence. Cells were maintained and passed as described above. Stock C225 and AG1478 was provided by of Dr. Robert Coffey. For drug treatments, growth media was aspirated off taking precaution not to disturb adherent cells. Next either C225 or AG1478 (AG1478 stock solution in DMSO) was diluted to appropriate concentrations of in warmed DMEM growth medium supplemented with 10% FBS, 1% PS. 10 ml of this diluted drug medium stock was then added to appropriate plates. Plates were then returned to the incubator and harvested at 0, 1, 2, 4, 8, 12, 24, or 48 hours. Lysate perparation for western blotting in and qRT-PCR experiments are described in those sections.

Standard histology

For immunohistochemistry, tissues were sectioned at 5.0 μm and stained for tumor proliferation markers (such as Ki67, p-His-H3 (m-phase), PCNA (S-phase), Dako Cytomation). All immunohistochemistry was performed using the Dako Cytomation, Envision + System – HRP Detection Kit. Tissue staining was carried out by Mr. Frank Revetta with the GI SPORE Tissue Core and evaluated by an expert pathologist, Dr. M. Kay Washington. Images were taken on a Zeiss axioskop and captured with CRI Nuance camera and software. Cells were counted with assistance of ImageJ software. Cells were scored as percent positive per field.

SiRNA experiments

All cells for SiRNA experiments were cultured as described above. Experiments were conducted in 6 well tissue culture treated dishes. All cells given SiRNA, either random or p27 specific, were cultured in 3.0 % serum as per manufacturers instructions. Control cells not treated with SiRNA were cultured in 10.0 % serum. Cells were tripsinized from large dishes as described above then resuspended in 10 ml total volume of supplemented DMEM media. Cells were transferred to 15ml conical tubes and centrifuged briefly to pellet cells. Media and tripsin were then aspirated off and cells were washed and resuspended in 5ml DPBS. Next, 100 ul of suspension was transferred to a micorcentrifuge tube and stained with trypan blue. Next, 15ul of trypan blue stained cells were pipetted into a hemocytometer to determine the concentration of cells in suspension. 500,000 cells were plated into each well on day zero. On day one, SiRNA was added to appropriate wells. The p27 and random smartpool sequence Accell SiRNA (Dharmacon, Thermo Scientific) were used for these procedures. 20 nmol lyophilized SiRNA was resuspended in 200ul 1x SiRNA buffer by gently pipetting 5 times then rocking for 30 min. SiRNA buffer was prepared by adding 30ml RNase-free water, 2.24 g KCl, 0.72g HEPES-free acid, 0.02g magnesium chloride $6H_2O$, 2ml freshly prepared 2.0 M KOH in a sterile 100 ml tube. The buffer was adjusted to a pH of 7.4 then sterile filtered and stored at $4\,^{o}C$ when not in use. SiRNA was diluted to 1 uM in 3.0% serum Accell delivery media (Dharmacon, Thermo Scientific). Next, 3.0 ml of appropriate SiRNA was added to appropriate wells. Cells were returned to incubator and checked daily to assess cell viability. On day four, pretreatment control, p27 SiRNA control, and random SiRNA control cells were harvested according to western blot protocol below.

C225 was added directly to appropriate wells for a total concentration of 5ug/ml on day four. On day five all remaining cells were harvested for western blotting as described below.

RNA isolation

In vitro samples were lysed in buffer RLT (provided with Quiagen RNeasy kit) from the RNeasy mini kit and transferred directly to the QIAschredder (Quiagen, cat. Number 79656) columns for homogenization. RNA was isolated using the RNeasy Mini column kit (Quiagen) according to the manufactures protocol with additional on column DNase treatment. All reagents for RNA isolation were obtained from the Vanderbilt University Molecular Biology Resource Core.

Reverse transcription reactions for real time PCR

QRT-PCR reactions were performed at the VU Microarray Shared Resource Core. RNA samples were quantitated using a Nanodrop spectrophotometer. For each sample 1-3 RT reactions were set up in a 96-well PCR plate. For each reaction, 0.35ug of starting RNA was added to 1ul of random hexamer primer (5'-NNNNNN-3' at 8ug/ul) and the volume was then adjusted to 18ul. The plate was heated in a thermal cycler for 5' at 70°C, cooled to 20°C for 10', and then held at 4°C. Samples were transferred to ice prior to addition of the PCR master mix. Master mix was made by combining per reaction 6.6ul of 5X First Strand Buffer, 3.3ul of 100mM DTT (both reagents are provided with the RT enzyme), 1.1ul 30X dNTPs (6mM final concentration of each dNTP), and 2.2ul of Superscript II Reverse Transcriptase (Invitrogen #18064-014). Each RT reaction received

12ul of Master Mix. Reactions were incubated for 2 hours at 42°C. A hydrolysis solution was made by combining equivalent amounts 1N NaOH and 0.5M EDTA, pH 8.0. Reactions were hydrolyzed with 20ul of hydrolysis solution and incubated at 70°C for 10 min followed by 20°C for 2 min. Following the incubation, 14ul of 1N HCl was added to each tube reaction to neutralize the reaction. Reactions were purified using Qiagen's PCR Purification Kit (#28106), following the manufacturers protocol. The cleaned up reactions were then quantitated by spectrophotometry and stored at -20°C.

Confocal immunofluorescence

All confocal specimens were imaged at the VUMC Shared Cell Imaging Core. Cells were grown on poly-L-lysine coated coverslips and treated with 5.0 ug/ul C225. Cells were washed in TBS, then fixed in freshly made 4.0% paraformaldehyde for 10 min. Coverslips were then washed with TBS and permeabilized in 0.2% Triton X-100 for five min. They were then rinsed three times in TBS. Coverslips were blocked in 10% goat serum, 1% BSA for one hour. Cells were incubated in p27 (Cat. Number 2552) or FoxO3a (Cat. Number 2497) antibodies from Cell Signaling diluted 1:1,000 in 1% BSA in TBS overnight at 4°C. Cells were washed in TBS and incubated with Oregon Green conjugated secondary antibody diluted 1:2,000 in 1% BSA in TBS for 45min and mounted with ProLong Gold with DAPI. Images were acquired with a Olympus FV-1000 confocal microscope and analyzed with Olympus Fluoview version 1.6a software.
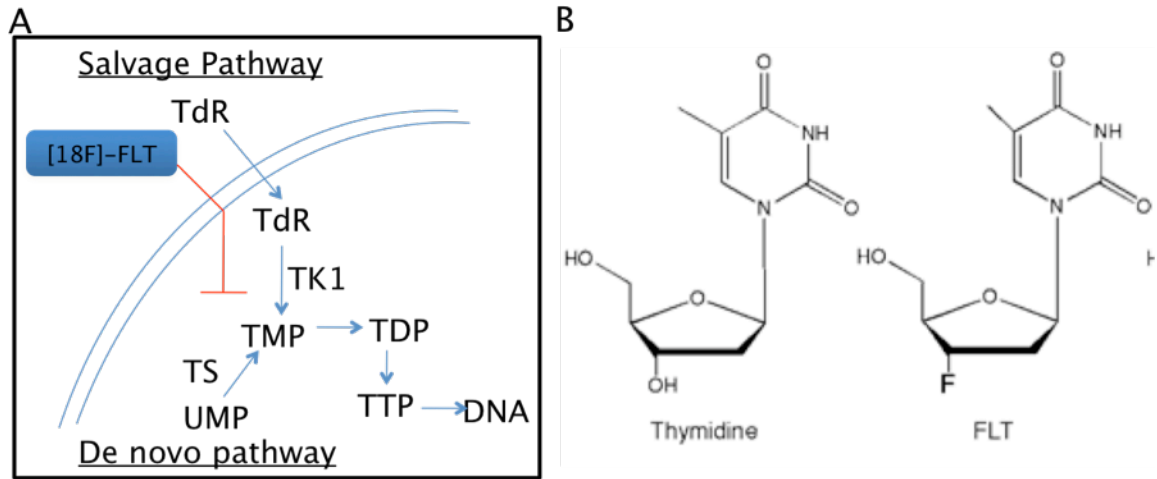
Cell culture western blot

Cells were harvested with CellLytic M lysis buffer supplemented with a protease inhibitor cocktail (Roche, Indianapolis, IN) and phosphates inhibitors 1 and 2 (Sigma) for *in vitro* assays. Total protein content was measured using the BCA assay kit (Biorad). 25ug total protein from each sample was loaded into 7.5-12% SDS-poly-acrylamide gels and resolved by electrophoresis at 125-175 volts prior to transferring to PVDF membranes. Transfers were carried out a 70 mA in an ice bath overnight. Membranes rinsed briefly in distilled water then were blocked overnight at 4°C in tris-buffered saline 0.1% Tween-20 (TBST) containing 5% w/v dry milk powder. Subsequently, membranes were washed then incubated with primary antibodies diluted 1:1,000 in TBST containing 3% w/v bovine serum albumin overnight at 4 °C. Primary antibodies used were Cyc D1(Cell Signaling, #2926), Cyc D3(Cell Signaling, #2936), Cyc E(Cell Signaling, #4129) Cdk 2(Cell Signaling, #2546)/4(Cell Signaling, #2906)/6(Cell Signaling, #3136), p21 (Cell Signaling, #2946), p27 (Cell Signaling, #2552), p15 (Cell Signaling, #4822), p16 (Cell Signaling, #4824), p53(Cell Signaling, #9283) , phospho-p53 Ser 15 (Cell Signaling, #9284), ERK1/2 (Cell Signaling, #4695), phospho p44/42-ERK1/2 Thr 202 Tyr 204 (Cell Signaling, #4370), phospho-MEK1/2 Ser 217/221 (Cell Signaling, #9154), total EGFR (Cell Signaling, #4405), phospho-EGFR Tyr 1173(Cell Signaling, #4407), phospho-EGFR Tyr 1148 (Cell Signaling, #4404), Ras (Cell Signaling, #3965), total AKT (Cell Signaling, #9272), phospho-AKT Thr 308 (Cell Signaling, #4056), phospho-AKT Ser 473 (Cell Signaling, #4058), PCNA (Cell Signaling, #2586), phospho-Rb Ser 795 (Cell Signaling, #9301), phospho-Rb Ser 807/811 (Cell Signaling, #9308), PTEN (Cell Signaling, #9559), phospho-PTEN (), FoxO3a (Cell Signaling, #4976), phospho-

FoxO3a Thr 32 (, phospho-FoxO3a Ser 253 (from Cell Signaling, and TK1 from Abcam.

The ladder used for determination of protein size was the PageRuler Plus prestained

protein ladder from Fermentas (cat. # SM1811) This was followed by incubation for 1 h

at room temperature with the appropriate horseradish peroxidase-conjugated secondary

antibody diluted 1:2,000 in TBST containing 3% w/v dry milk powder. Enhanced

chemiluminescence (ECLplus; GE Healthcare-Biosciences, Piscataway, NJ, USA) was

used for detection on a Xenogen IVIS system. Bands corresponding to various proteins of

interest were quantified using Living Imaging software.

Tissue WB analysis

Protein lysates were prepared by homogenizing fresh frozen tissue in cold

CellLytic-MT (Sigma) buffer containing a cocktail of protease inhibitors (Sigma). The

homogenized lysates were cleared by centrifugation and the total protein was quantified

in a BCA assay. For western blotting, samples were processed as described above and

blotted with TK1 mouse monoclonal antibody (abcam).

FIGURES

Figure 1. (A)Salvage and *de novo* pathways of thymidine utilization. Adapted from
Bading and Shields 2008. (B) Structures of FLT and thymidine showing difference in 2'
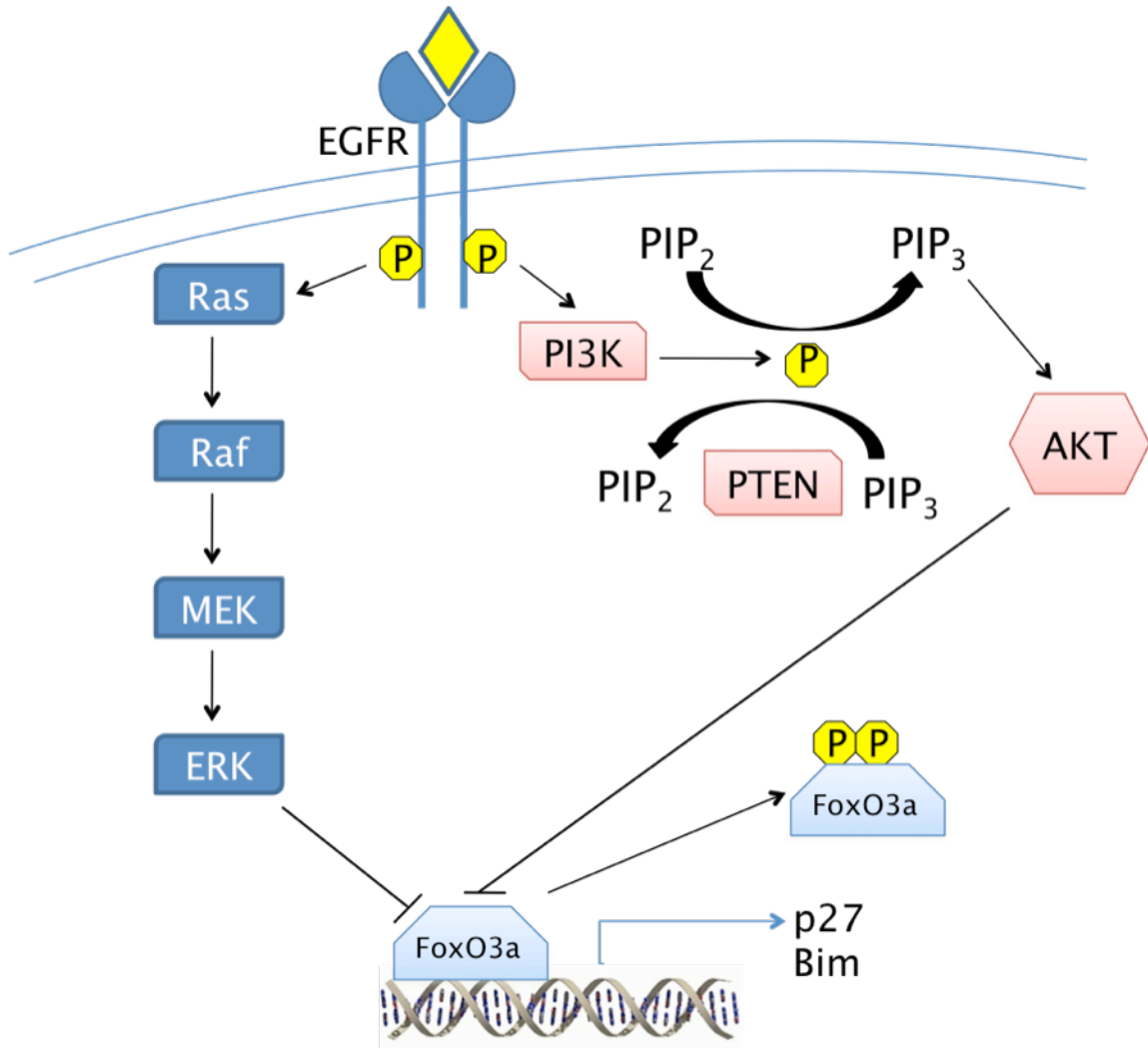carbon with 18F functionalization.

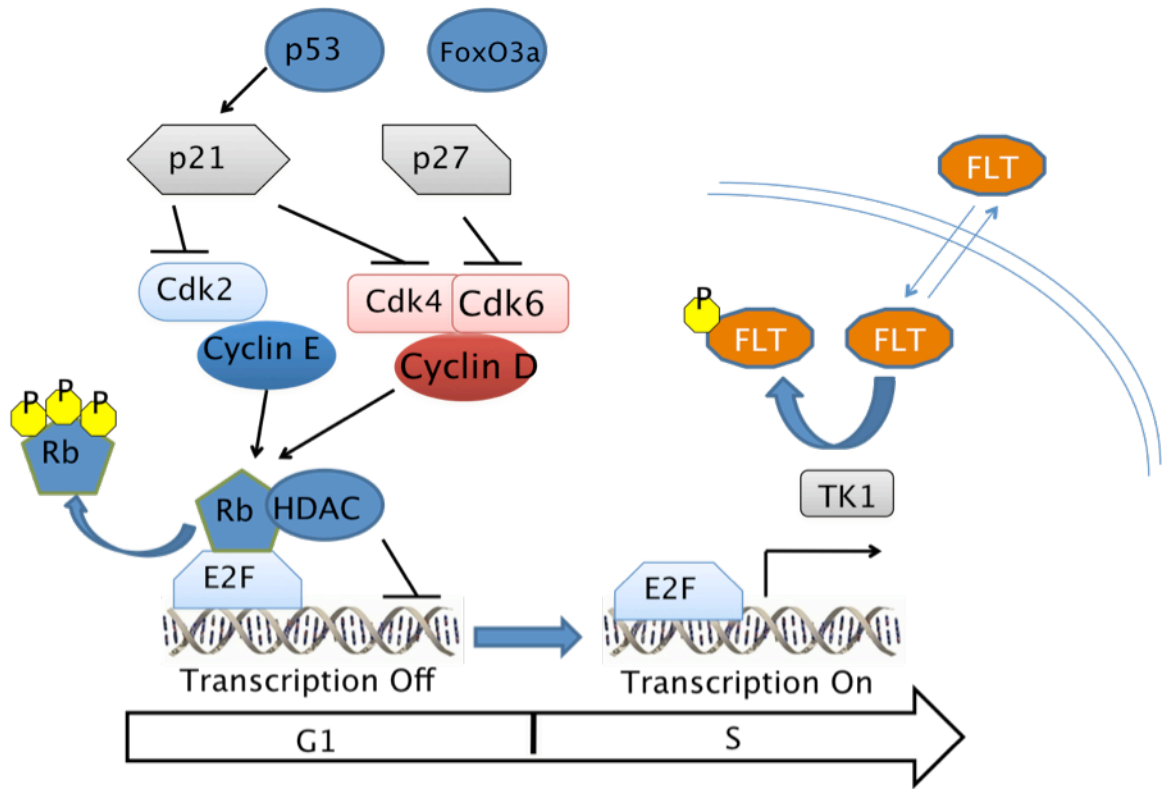Figure 2. EGFR signaling via MAPK and or AKT pathways regulates transcription of p27 and Bim through FoxO3a.

Figure 3. Cell cycle regulatory proteins govern TK1 expression via the E2F transcription factor at the G1/S transition. TK1 is ultimately responsible for phosphorylation and retention of FLT.
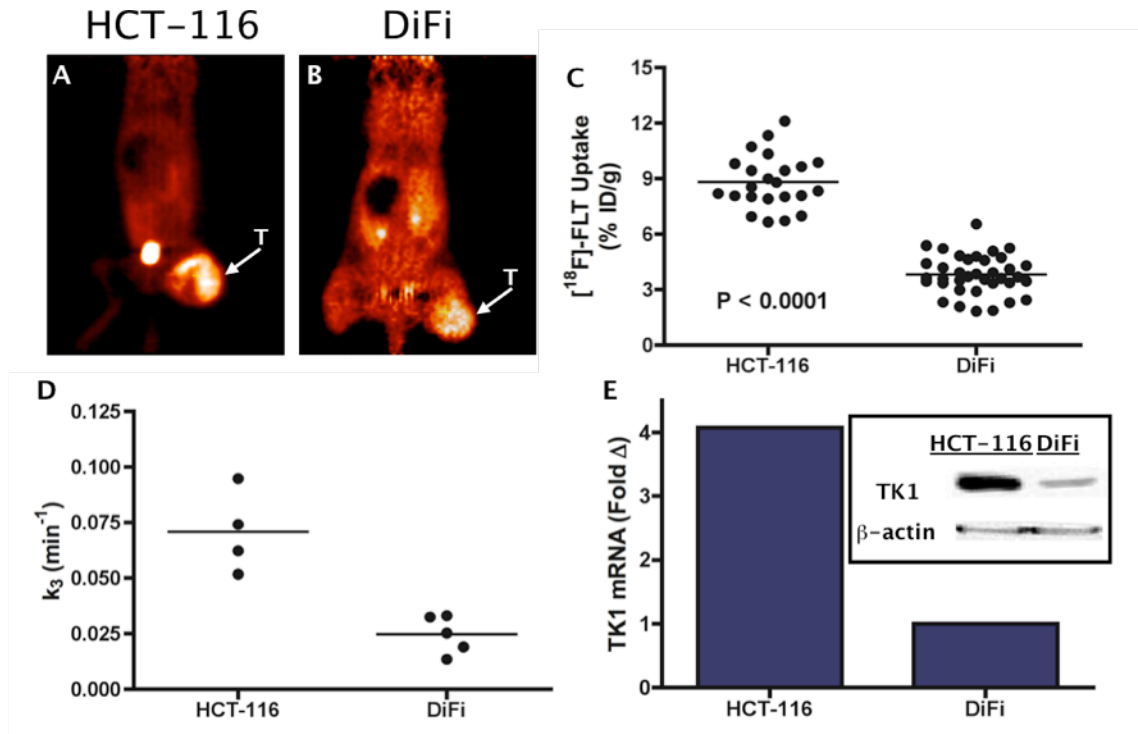
Figure 4. Uptake of [^{18}F]-FLT discriminates HCT116 from DiFi human CRC cell line xenografts. Representative [^{18}F]-FLT images of (A) HCT-116 and (B) DiFi xenograft bearing mice. "T"denotes tumor. Quantification of static (%ID/g, C) and dynamic (k3, D) measurements, 60 min tracer uptake. (E) relative TK1 mRNA expression fold change from baseline levels (average of n = 2 animals/cell line xenograft) by qRT-PCR and (inset) relative TK1 protein levels by western blot analysis.
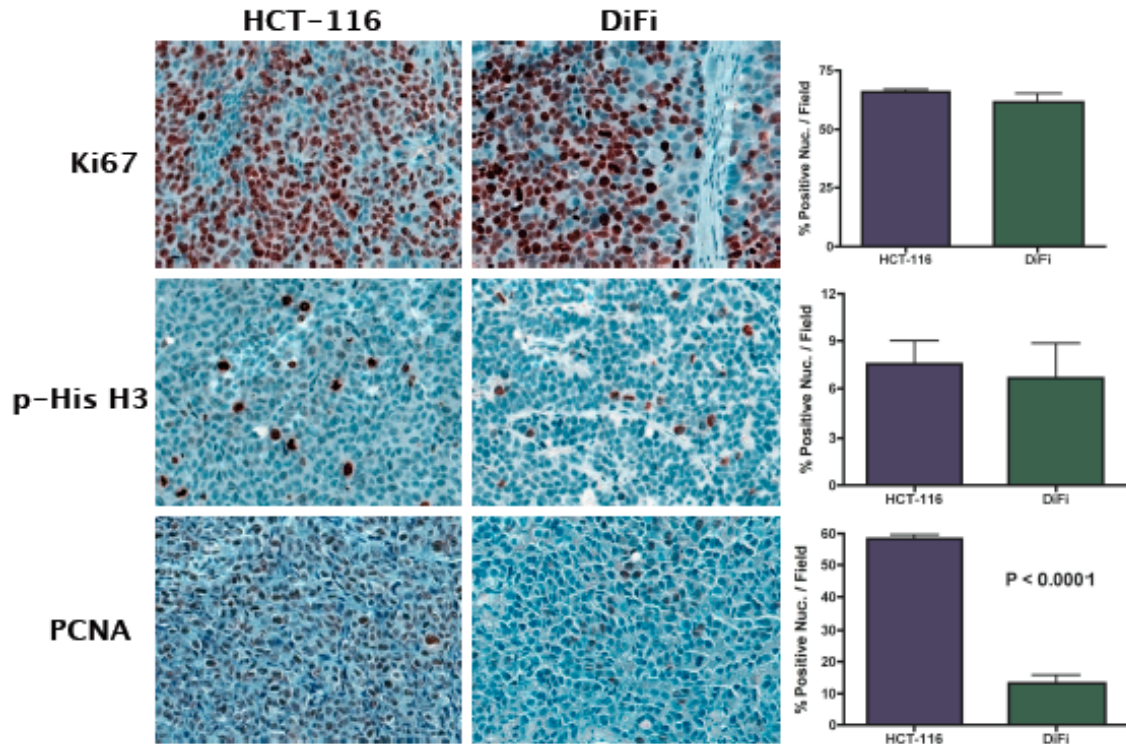
Figure 5. Immunostaining of HCT116 and DiFi human CRC cell line xenograft tissues. Levels of both Ki67 and p-His-H3 staining are similar across representative HCT116 and DiFi tumor tissues. PCNA staining illustrates a significantly higher fraction of HCT116 cells in S-phase than DiFi cells.
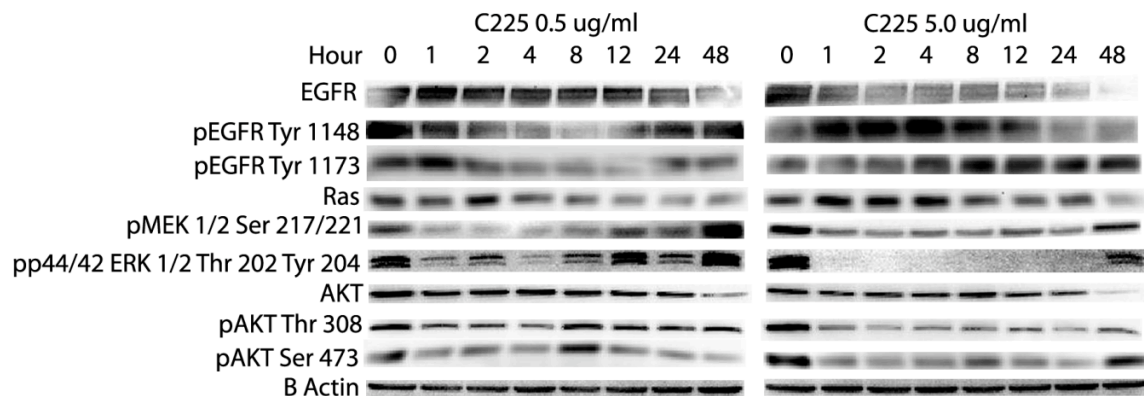

Figure 6. Western blot analysis of effect of C225 on EGFR, and MAPK and AKT signaling proteins in DiFi cells at two concentrations of C225.
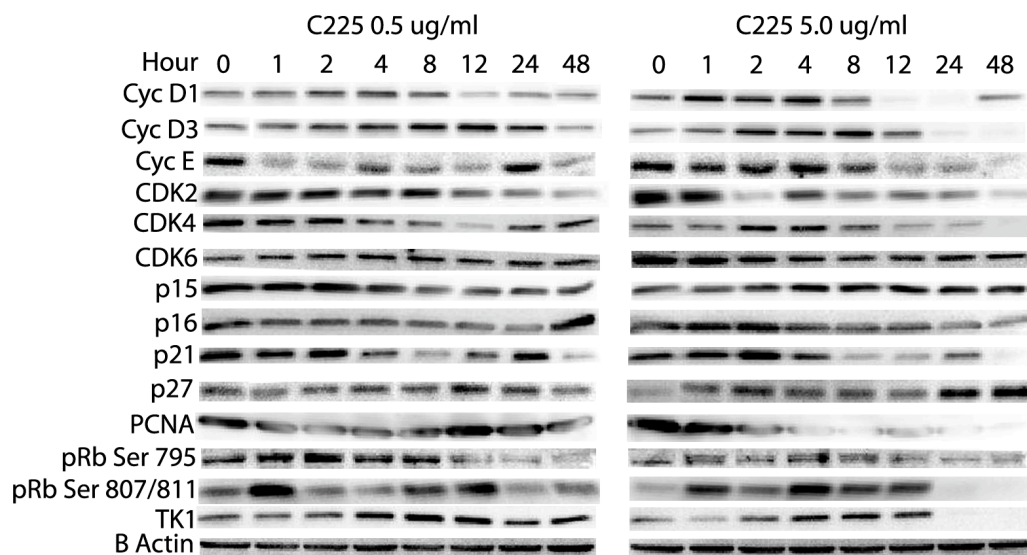
Figure 7. Effect of C225 on cell cycle regulation of TK1 in DiFi cells. WB analysis of G1-S transition molecules at two concentrations of C225 exposure.
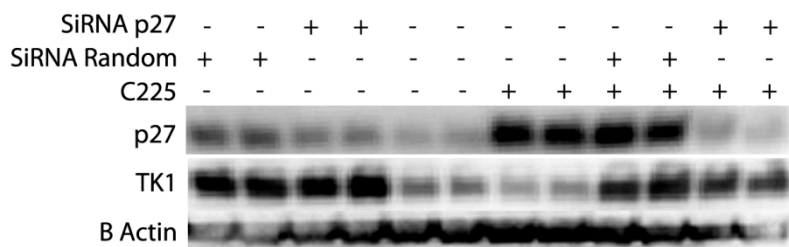

Figure 8. Western blot of C225 (24 hours exposure) and SiRNA (72 hours exposure) treated DiFi cells showing inverse relationship between levels of p27 and TK1 protein.
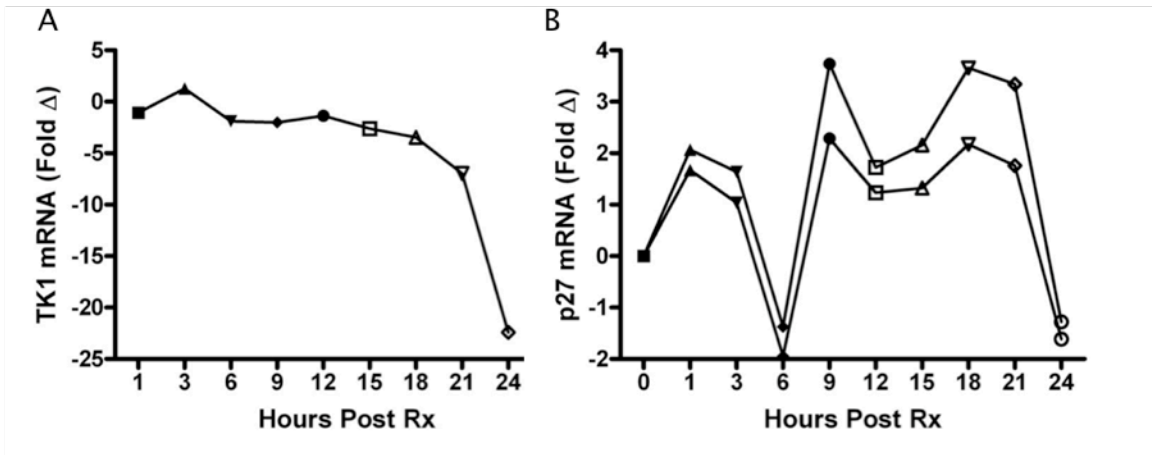
Figure 9. (A) qRT-PCR analysis of TK1 and (B) p27 mRNA fold change relative to baseline after exposure to C225 at various time points.
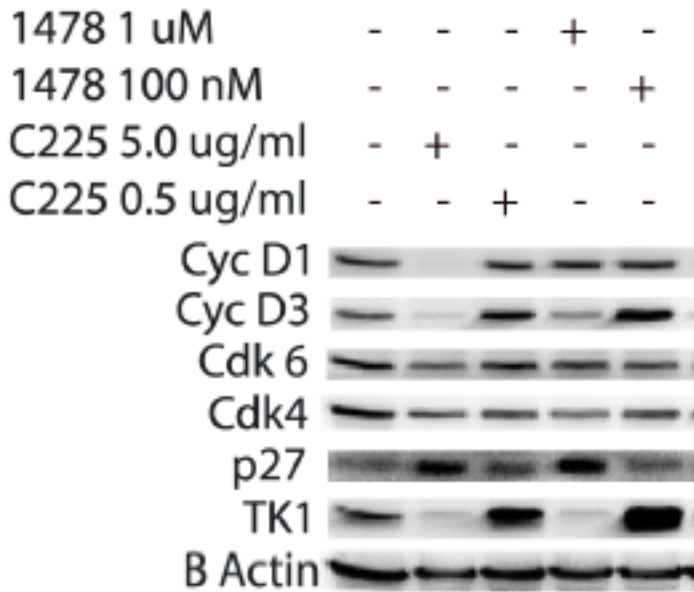

Figure 10. Comparison of mAb C225 to small molecule TKI AG1478 on cell cycle regulation of TK1 in DiFi cells. WB analysis of G1-S transition molecules at two concentrations of C225 exposure and AG1478.
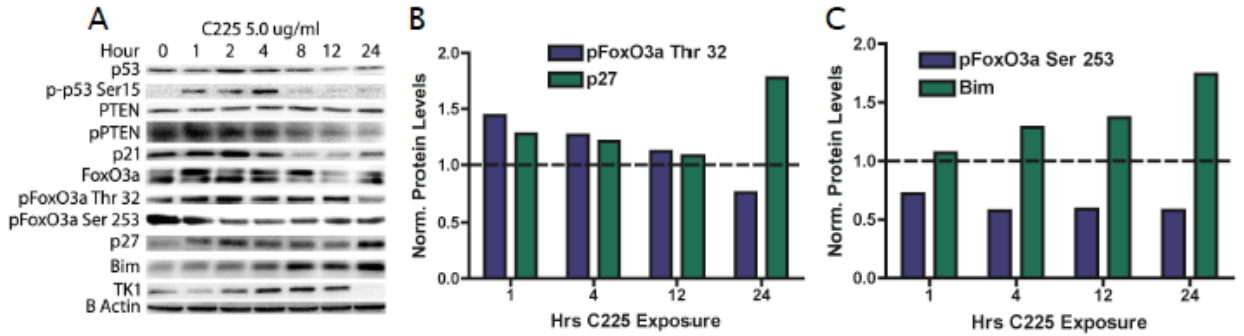
Figure 11. C225-mediated induction of p27 in DiFi cells is regulated by forkhead signaling. (A) WB analysis of DiFi cells treated with C225 over time illustrate coincident loss of activated p53, activated PTEN, and p21 beyond 4 hrs of C225 exposure. In contrast, induction of p27, which occurs concomitantly with reduced TK1, occurs in concert with reduced pFoxO3a Thr 32 (B). Additionally, induction of Bim precedes p27 induction and is closely associated with loss of pFoxO3a Ser 253 (C). Dashed lines indicate baseline protein levels.
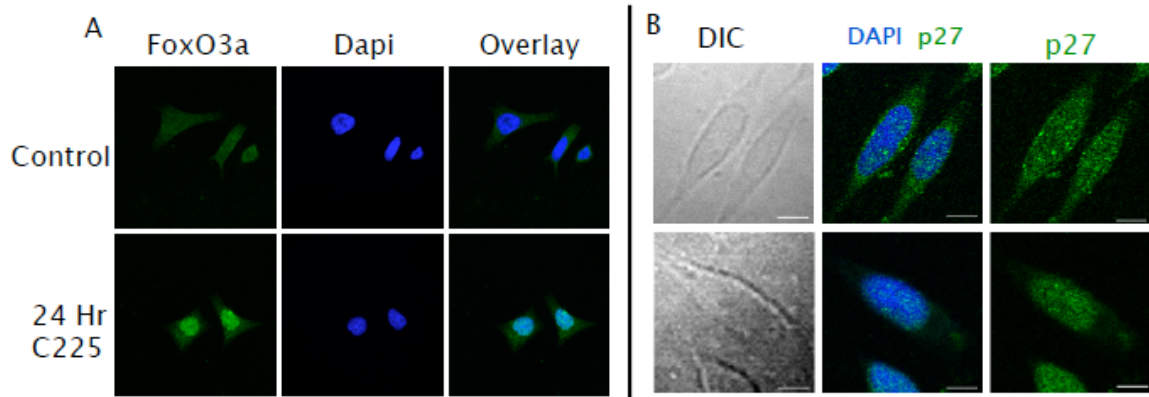
Figure 12. (A) C225-induced FoxO3a is primarily nuclear in DiFi cells as assessed by confocal microscopy. Low-level FoxO3a in vehicle treated DiFi cells is an equal mixture of cytosolic and nuclear protein. (B) C225-induced p27 is primarily nuclear in DiFi cells as assessed by confocal microscopy. Low-level p27 in vehicle treated DiFi cells is an equal mixture of cytosolic and nuclear protein.
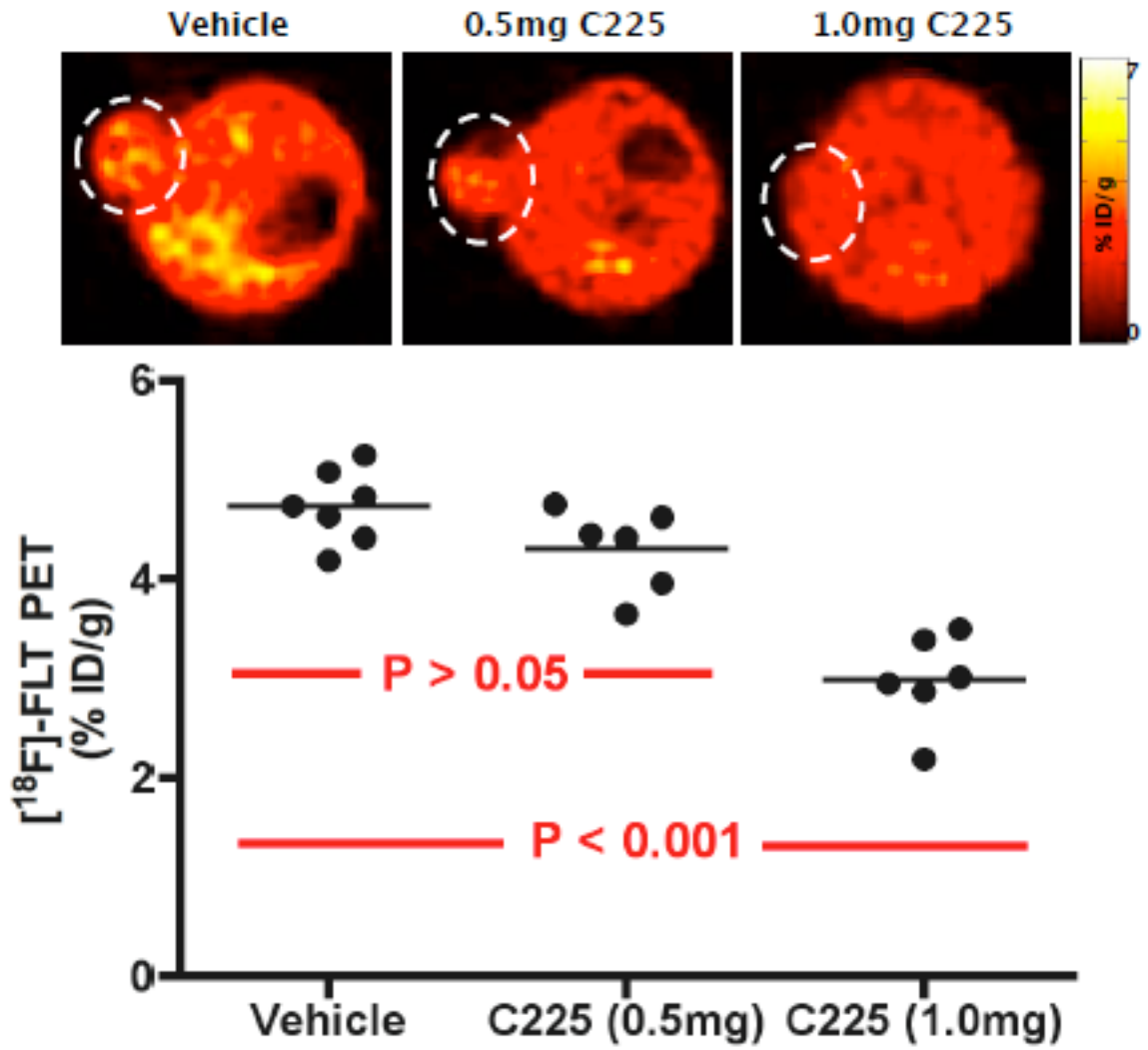
Figure 13. [18F]-FLT PET to assess dose response in DiFi xenografts. A 1.0 mg/ injection dose, but not a 0.5 mg/injection dose will reduce [18F]-FLT uptake in this model.

REFERENCES

1. Arner, E.S. and S. Eriksson, *Mammalian deoxyribonucleoside kinases.* Pharmacol Ther, 1995. **67**(2): p. 155-86.

2. Bradshaw, H.D., Jr., *Molecular cloning and cell cycle-specific regulation of a functional human thymidine kinase gene.* Proc Natl Acad Sci U S A, 1983. **80**(18): p. 5588-91.

3. Kreidberg, J.A. and T.J. Kelly, *Genetic analysis of the human thymidine kinase gene promoter.* Mol Cell Biol, 1986. **6**(8): p. 2903-9.

4. Travali, S., et al., *Role of the promoter in the regulation of the thymidine kinase gene.* Mol Cell Biol, 1988. **8**(4): p. 1551-7.

5. Arcot, S.S., E.K. Flemington, and P.L. Deininger, *The human thymidine kinase gene promoter. Deletion analysis and specific protein binding.* J Biol Chem, 1989. **264**(4): p. 2343-9.

6. Kim, Y.K., et al., *Sequences contained within the promoter of the human thymidine kinase gene can direct cell-cycle regulation of heterologous fusion genes.* Proc Natl Acad Sci U S A, 1988. **85**(16): p. 5894-8.

7. Merrill, G.F., S.D. Hauschka, and S.L. McKnight, *tk Enzyme expression in differentiating muscle cells is regulated through an internal segment of the cellular tk gene.* Mol Cell Biol, 1984. **4**(9): p. 1777-84.

8. Stewart, C.J., M. Ito, and S.E. Conrad, *Evidence for transcriptional and post-transcriptional control of the cellular thymidine kinase gene.* Mol Cell Biol, 1987. **7**(3): p. 1156-63.

9. Schlosser, C.A., et al., *Cell cycle-dependent regulation of thymidine kinase activity introduced into mouse LMTK- cells by DNA and chromatin-mediated gene transfer.* Proc Natl Acad Sci U S A, 1981. **78**(2): p. 1119-23.

10. Johnson, L.F., L.G. Rao, and A.J. Muench, *Regulation of thymidine kinase enzyme level in serum-stimulated mouse 3T6 fibroblasts.* Exp Cell Res, 1982. **138**(1): p. 79-85.

11. Sherley, J.L. and T.J. Kelly, *Regulation of human thymidine kinase during the cell cycle.* J Biol Chem, 1988. **263**(17): p. 8350-8.

12. Meric, F. and K.K. Hunt, *Translation initiation in cancer: a novel target for therapy.* Mol Cancer Ther, 2002. **1**(11): p. 971-9.

13. Kauffman, M.G. and T.J. Kelly, *Cell cycle regulation of thymidine kinase: residues near the carboxyl terminus are essential for the specific degradation of the enzyme at mitosis.* Mol Cell Biol, 1991. **11**(5): p. 2538-46.

14.   Gan, T.E., J.L. Brumley, and M.B. Van der Weyden, *Human thymidine kinase. Purification and properties of the cytosolic enzyme of placenta.* J Biol Chem, 1983. **258**(11): p. 7000-4.

15.   Bradshaw, H.D., Jr. and P.L. Deininger, *Human thymidine kinase gene: molecular cloning and nucleotide sequence of a cDNA expressible in mammalian cells.* Mol Cell Biol, 1984. **4**(11): p. 2316-20.

16.   Segura-Pena, D., et al., *Binding of ATP to TK1-like enzymes is associated with a conformational change in the quaternary structure.* J Mol Biol, 2007. **369**(1): p. 129-41.

17.   Nugent, K.P., et al., *Randomized controlled trial of the effect of sulindac on duodenal and rectal polyposis and cell proliferation in patients with familial adenomatous polyposis.* Br J Surg, 1993. **80**(12): p. 1618-9.

18.   Manning, H.C., et al., *Molecular imaging of therapeutic response to epidermal growth factor receptor blockade in colorectal cancer.* Clin Cancer Res, 2008. **14**(22): p. 7413-22.

19.   Shields, A.F., *PET imaging with 18F-FLT and thymidine analogs: promise and pitfalls.* J Nucl Med, 2003. **44**(9): p. 1432-4.

20.   Mankoff, D.A. and J.F. Eary, *Proliferation imaging to measure early cancer response to targeted therapy.* Clin Cancer Res, 2008. **14**(22): p. 7159-60.

21.   Sohn, H.J., et al., *[18F]Fluorothymidine positron emission tomography before and 7 days after gefitinib treatment predicts response in patients with advanced adenocarcinoma of the lung.* Clin Cancer Res, 2008. **14**(22): p. 7423-9.

22.   Eriksson, S., et al., *Comparison of the substrate specificities of human thymidine kinase 1 and 2 and deoxycytidine kinase toward antiviral and cytostatic nucleoside analogs.* Biochem Biophys Res Commun, 1991. **176**(2): p. 586-92.

23.   Bading, J.R. and A.F. Shields, *Imaging of cell proliferation: status and prospects.* J Nucl Med, 2008. **49 Suppl 2**: p. 64S-80S.

24.   Rasey, J.S., et al., *Validation of FLT uptake as a measure of thymidine kinase-1 activity in A549 carcinoma cells.* J Nucl Med, 2002. **43**(9): p. 1210-7.

25.   Francis, D.L., et al., *Potential impact of [18F]3'-deoxy-3'-fluorothymidine versus [18F]fluoro-2-deoxy-D-glucose in positron emission tomography for colorectal cancer.* Eur J Nucl Med Mol Imaging, 2003. **30**(7): p. 988-94.

26.   Leyton, J., et al., *In vivo biological activity of the histone deacetylase inhibitor LAQ824 is detectable with 3'-deoxy-3'-[18F]fluorothymidine positron emission tomography.* Cancer Res, 2006. **66**(15): p. 7621-9.

27. Barthel, H., et al., *The uptake of 3'-deoxy-3'-[18F]fluorothymidine into L5178Y tumours in vivo is dependent on thymidine kinase 1 protein levels.* Eur J Nucl Med Mol Imaging, 2005. **32**(3): p. 257-63.

28. Linggi, B. and G. Carpenter, *ErbB receptors: new insights on mechanisms and biology.* Trends Cell Biol, 2006. **16**(12): p. 649-56.

29. Coffey, R.J., Jr., et al., *Transforming growth factor alpha and beta expression in human colon cancer lines: implications for an autocrine model.* Cancer Res, 1987. **47**(17): p. 4590-4.

30. Yang, J.Y. and M.C. Hung, *A new fork for clinical application: targeting forkhead transcription factors in cancer.* Clin Cancer Res, 2009. **15**(3): p. 752-7.

31. Mitsuuchi, Y., et al., *The phosphatidylinositol 3-kinase/AKT signal transduction pathway plays a critical role in the expression of p21WAF1/CIP1/SDI1 induced by cisplatin and paclitaxel.* Cancer Res, 2000. **60**(19): p. 5390-4.

32. Yang, J.Y., et al., *ERK promotes tumorigenesis by inhibiting FOXO3a via MDM2-mediated degradation.* Nat Cell Biol, 2008. **10**(2): p. 138-48.

33. Olive, M., et al., *Characterization of the DiFi rectal carcinoma cell line derived from a familial adenomatous polyposis patient.* In Vitro Cell Dev Biol, 1993. **29A**(3 Pt 1): p. 239-48.

34. Khambata-Ford, S., et al., *Expression of epiregulin and amphiregulin and K-ras mutation status predict disease control in metastatic colorectal cancer patients treated with cetuximab.* J Clin Oncol, 2007. **25**(22): p. 3230-7.

35. Bradbury, M.S., et al., *Dynamic small-animal PET imaging of tumor proliferation with 3'-deoxy-3'-18F-fluorothymidine in a genetically engineered mouse model of high-grade gliomas.* J Nucl Med, 2008. **49**(3): p. 422-9.

36. Nowak, S.J. and V.G. Corces, *Phosphorylation of histone H3: a balancing act between chromosome condensation and transcriptional activation.* Trends Genet, 2004. **20**(4): p. 214-20.

37. Moldovan, G.L., B. Pfander, and S. Jentsch, *PCNA, the maestro of the replication fork.* Cell, 2007. **129**(4): p. 665-79.

38. Alkarain, A., R. Jordan, and J. Slingerland, *p27 deregulation in breast cancer: prognostic significance and implications for therapy.* J Mammary Gland Biol Neoplasia, 2004. **9**(1): p. 67-80.

39. Wickenden, J.A., et al., *Colorectal cancer cells with the BRAF(V600E) mutation are addicted to the ERK1/2 pathway for growth factor-independent survival and repression of BIM.* Oncogene, 2008. **27**(57): p. 7150-61.